THE ASTROPHYSICAL JOURNAL, 410:534–542, 1993 June 20

THE NARROW-LINE REGION OF HIGH-LUMINOSITY ACTIVE GALACTIC NUCLEI[1]

BEVERLEY J. WILLS,[2,3] H. NETZER,[4,5] M. S. BROTHERTON,[2] MINGSHENG HAN,[2] D. WILLS,[2] J. A. BALDWIN,[5] G. J. FERLAND,[6] AND I. W. A. BROWNE[7]

Received 1992 September 15; accepted 1992 December 17

ABSTRACT

We have made high signal-to-noise spectroscopic observations of seven radio-loud quasars with the Faint Object Spectrograph on the *Hubble Space Telescope* and from the ground at McDonald Observatory and at Kitt Peak National Observatory. The resolution is 300–400 km s^{-1} over the wavelength range 1000–8500 Å, enabling us to separate the broad and narrow components of the emission lines. This is the first study of the optical and UV narrow lines in such high-luminosity active galactic nuclei (AGNs).

The most important and striking observational result is the relative weakness of the narrow ultraviolet lines, assuming that they have the same widths as the narrow [O III] λ5007 emission lines. We do not have a single definite detection of a narrow UV line in any of the seven quasars. We have measured all the strong optical narrow lines and have derived upper limits to the strengths of narrow lines in the UV. The latter are much weaker than predicted by dust-free photoionization models and also weaker than those typically seen in Seyfert 2 galaxies and narrow-line radio galaxies. There is direct evidence for the presence of dust with significant reddening, typically $E(B-V) \sim 0.5$. A comparison of our sample with the previously observed Seyfert 2s (Kinney et al.) shows that two explanations for the reddening are needed. One is simple foreground reddening, presumably in the host galaxy. However some narrow-line spectra show an unsually weak Lyα/Hβ intensity ratio, but apparently case B Hα/Hβ. We interpret this as the result of dust inside the narrow line clouds and show model calculations to support this claim. These and other calculations presented in this paper are used to argue that much of the narrow-line region in the high-luminosity objects lies well beyond the nucleus.

Subject headings: galaxies: active — galaxies: nuclei — galaxies: Seyfert — quasars: general — ultraviolet: galaxies

1. INTRODUCTION

With the successful operation of the Faint Object Spectrograph on the *Hubble Space Telescope* (*HST*) it has become possible, for the first time, to attempt to resolve the narrow ultraviolet resonance lines of quasars' narrow-line regions (NLRs) and to measure their strength, even in the presence of the strong broad emission lines. Such measurements of low-redshift quasars were not possible previously because of the lower sensitivity and the poorer wavelength resolution of *IUE*. In the case of ground-based spectroscopy of high-redshift objects we are limited by the lack of observations of the narrow forbidden lines, hydrogen Balmer, and helium lines that are redshifted beyond ~1 μm, and by strong absorption lines near the peak emission of the strong ultraviolet lines. Thus only a handful of broad-line objects have been studied in this way (NGC 4151 with the Hopkins Ultraviolet Telescope [Kriss et al. 1992], MC 1331+170 by Carswell et al. [1991]), 3C 390.3 [Netzer 1982; Clavel & Wamsteker 1987], 3C 351 [Netzer, Wills, & Wills 1982], and the Kinney et al. 1991 sample to be discussed later).

Measurement of the complete narrow-line spectrum over a wide wavelength range in the same object allows several important and unique investigations. Because the NLR is thought to be of lower density (10^3–10^6 cm^{-3}) than the broad-line region (BLR, 10^9–10^{11} cm^{-3}), optical depth effects and collisional excitation are less complex, making it easier to predict the spectrum emitted by the photoionized gas. A comparison with the observed spectrum could simultaneously constrain the physical conditions in the emission-line gas, its covering factor, filling factor, and the ionizing continuum seen by the NLR. However, we must first understand the effects of dust.

Active galactic nuclei (AGNs) probably arise from the merging of gas-rich galaxies (Kormendy & Sanders 1992). Plumes and other gaseous signatures of tidal disruption are revealed in deep high-resolution images at optical and radio wavelengths. Extended regions of ionized gas are frequently detected around radio-loud as well as radio-quiet QSOs (Heckman et al. 1991a, b; Bremer et al. 1992). Thanks to *IRAS* we now appreciate that dust is very important energetically—many lower luminosity AGNs, and some of QSO-like luminosity, emit most power in the infrared, from dust heated by luminous stars or by a powerful nuclear continuum. So the potential for significant dust absorption and scattering is clearly present, although in the interests of oversimplicity this has often been overlooked (see the warnings by MacAlpine

[1] Based on observations with the NASA/ESA *Hubble Space Telescope*, obtained at the Space Telescope Science Institute, which is operated by the Association of Universities for Research in Astronomy, Inc., under NASA contract NAS 5-26555.

[2] McDonald Observatory and Astronomy Department, University of Texas at Austin, Austin, TX 78712.

[3] Visiting Astronomer, Kitt Peak National Observatory, National Optical Astronomy Observatories, operated by the Association of Universities for Research in Astronomy, Inc., under contract with the National Science Foundation.

[4] Department of Physics and Astronomy, Tel Aviv University, Tel Aviv 69978, Israel.

[5] Cerro-Tololo Inter-American Observatory, P.O. Box 26732, Tucson, AZ 85726.

[6] Institute of Astronomy, Cambridge, UK and the Royal Greenwich Observatory, UK on leave from the Department of Physics and Astronomy, University of Kentucky, Lexington, KY 40506-0055.

[7] University of Manchester Nuffield Radio Astronomy Laboratories, Jodrell Bank, Macclesfield, Cheshire, SK11 9DL, England.

1985; Ferland & Netzer 1979). Dust is an essential ingredient in unified schemes, where its presence can mask or scatter light from a luminous QSO nucleus (Rowan-Robinson 1977; Antonucci 1992; Kinney et al. 1991).

We are carrying out a program to obtain quasi-simultaneous ultraviolet, optical, and infrared spectra of a sample of about 50 quasars selected by extended radio luminosity to investigate relations between emission lines, X-ray, UV to IR continuum and radio emission, partly with a view to understanding the probably axisymmetric inner regions of quasars. Here we derive narrow-line spectra for the first available seven high-luminosity quasars and compare these with theoretical expectations and with the pure narrow-line spectra of Seyfert 2 and narrow line radio galaxies (NLRGs) (Ferland & Osterbrock 1986 [FO86]). In § 2 we describe our observations and in § 3 we present and tabulate the new results obtained for the narrow emission lines. Section 4 confronts our new data with present theories and discusses the implications for the size and composition of the NLR. Our conclusions are briefly summarized in § 5.

2. OBSERVATIONS AND REDUCTIONS

2.1. *HST Spectrophotometry*

Spectra from rest wavelengths below Lyα to observed wavelengths above the atmospheric cutoff near 3200 Å were obtained with *HST*'s Faint Object Spectrograph (FOS) in the high-resolution mode ($R = 1300$). A log of the observations is given in Table 1A. The blue digicon detector (BL) was used with the G130H grating centered at 1300 Å, and the red digicon detector (RD) with the gratings G190H, G270H, and G400H centered at 1900, 2700, and 4000 Å (Ford & Hartig 1990; Kinney 1992). Each digicon spectrum covers 512 diodes, obtained in 0.25 diode substeps (pixels) with an overscan of 5 diodes. Dispersions for the above grating setups are 0.25, 0.36, 0.51, and 0.75 Å pixel^{-1}. The 4.″3 × 4.″3 aperture was used for maximum throughput (about 0.5–0.7 from 1300 to 4000 Å). In the direction perpendicular to the dispersion this aperture is effectively limited to 1.″4 by the length of the digicon diodes. Centering and tracking is accurate to within ~0.″1, so spectral resolution is limited by the spectrograph itself and by the point-spread function of *HST*. The effective resolution for a point source is 1.5 diodes FWHM—or 6 pixels (i.e., ~350 km s^{-1}). The spectra are also affected by geomagnetic image motion (GIM)—image shifts resulting from the changing angle between the Earth's magnetic field and that of the Digicon, as the spacecraft orbits. Data are read out at 2 and 4 minute intervals for the red and blue digicons, respectively—a small fraction of the 90 minute orbit. The exposure times were estimated to give a signal-to-noise ratio of at least 8.5 per pixel in the continuum, in the region of important emission lines (Lyα, C IV λ1549, C III] λ1909 and Mg II λ2798). These estimates were based on a standard quasar spectrum derived from *IUE* and McDonald Observatory spectrophotometry of several radio-loud quasars. This results in a continuum signal-to-noise ratio of at least 21 per resolution element in the continuum and, of course, larger than this in the emission lines.

Standard calibration was by the CALFOS task in the IRAF/STSDAS package. This task corrects the raw counts to flux density. It takes into account diodes that have been disabled at the spacecraft, corrects for the GIM wavelength shifts, subtracts a default instrumental background, divides by a normalized flat field derived from observations of white dwarf stars obtained closest in time to the quasar observations, and computes a wavelength scale accurate to about 0.1 diodes. On rare occasions narrow emission spikes were observed in the data that were clearly not intrinsic to the quasar—they were not repeatable in the 2-minute data segments, and so were removed by interpolation. In addition noisy or dead diodes unknown before the actual observation time were found in our spectra with the characteristic width of 20 pixels—a result of the substepping and overscanning (the electron beam steps the spectrum sequentially over 4 × 5 = 20 quarter-diodes).

2.2. *Optical Spectrophotometry*

Quasi-simultaneous spectrophotometry was obtained using the Large Cassegrain Spectrograph (LCS) with either a thinned TI 800 × 800 CCD or a thick CRAF 1024 × 1024 CCD at the f/18 focus of the McDonald Observatory 2.7 m telescope. A log of these observations is given in Table 1B, with information on dates, instrumentation, and weather conditions. A low-resolution grating (300 grooves mm^{-1}) was used with two or three grating settings to extend the spectrum to at least 8500 Å, and with significant overlap with the FOS spectra in the blue to check for any time-variability, weather permitting. Short exposures with a large projected slit width of typically 8″ were made for spectrophotometry, and longer exposures with a 2″ slit were made for best signal-to-noise and wavelength resolution of about 10.5 Å FWHM ($R = 380$–750). These observations were supplemented where possible by observations with a 600 line mm^{-1} grating (5–6 Å FWHM) made for a parallel investigation of broad emission-line profiles. The quasars and most standard stars were observed near the zenith (air masses < 1.5). The estimated absolute calibration uncertainties are ~5%. Atmospheric absorption bands were carefully removed by division by the spectrum of hot stars (usually

TABLE 1A

LOG OF *HST* OBSERVATIONS

Target	Detector	Grating	Exp Time (minutes)	Date (UT)	Root Name (Y0PE)
PKS0403-13	RD	G190H	23.5	1991 Oct 11	0202
	RD	G270H	12.6	1991 Oct 11	0203
	RD	G400H	08.9	1991 Oct 11	0204
3C175	RD	G190H	28.2	1991 Dec 03	0302
	RD	G270H	12.0	1991 Dec 03	0303
	RD	G400H	08.1	1991 Dec 03	0304
3C215	RD	G190H	30.5	1992 May 02	0602
	RD	G190H	30.5	1992 May 02	0603
	RD	G190H	30.5	1992 May 02	0604
	RD	G270H	12.1	1992 May 02	0605
	RD	G270H	12.0	1992 May 02	0606
	RD	G400H	18.9	1992 May 02	0607
3C254	RD	G190H	18.5	1992 Apr 16	0802
	RD	G190H	18.5	1992 Apr 16	0803
	RD	G270H	22.9	1992 Apr 16	0804
	RD	G400H	19.2	1992 Apr 16	0805
3C263	RD	G190H	08.9	1991 Nov 06	0902
	RD	G270H	04.6	1991 Nov 06	0903
	RD	G400H	03.4	1991 Nov 06	0904
3C277.1	RD	G190H	33.1	1991 Nov 02	0A02
	RD	G270H	18.7	1991 Nov 02	0A03
	RD	G400H	14.4	1991 Nov 02	0A04
3C323.1	BL	G130H	19.2	1992 Apr 11	0C02
	BL	G130H	19.3	1992 Apr 11	0C03
	RD	G190H	06.4	1992 Apr 09	0D02
	RD	G270H	03.7	1992 Apr 09	0D03
	RD	G400H	02.6	1992 Apr 09	0D04

TABLE 1B

LOG FOR THE OPTICAL OBSERVATIONS

Name	Date (UT)			Wavelength Range (Å)[a]	Slit width (arcsec)	Exposure Time (sec)	Sky Conditions[b]		CCD[c]
0403-13	1991	Dec	31	4580 – 7297	7.5	1200	phot	2″	TI
	1992	Jan	1	4557 – 7275	2	1800		2″	TI
	1992	Jan	2	6264 – 8998	2	3600		2″	TI
	1992	Jan	2	6264 – 8998	5	1500	phot	2″	TI
3C175[d]	1991	Dec	31	4580 – 7297	7.5	1200	phot	2″	TI
	1992	Jan	1	4557 – 7275	2	1800		2″	TI
	1992	Jan	2	6264 – 8998	2	3600		2″	TI
	1992	Jan	2	6264 – 8998	5	1200	phot	2″	TI
	1992	Mar	10	3099 – 5814	2	2700	cloud	2–3″	TI
3C215	1992	Jan	1	4557 – 7275	7.5	1500	phot	2″	TI
	1992	Jan	5	4589 – 7301	2	3600		2″	TI
	1992	Feb	26[e]	4939 – 9500	2.4	3960		2–3″	TI
	1992	Feb	28[f]	5796 – 7201	2	8100		2–2.5″	TI
	1992	Feb	29[f]	6305 – 7694	2	5400		2–2.5″	TI
	1992	Mar	8	4597 – 7315	2	5400			TI
3C254	1992	Jan	1	4557 – 7275	2	1500		2″	TI
	1992	Jan	1	4557 – 7275	7.5	1500	phot	2″	TI
	1992	Apr	7	4583 – 7338	2	3600		2″	CRAF
	1992	Apr	7	4583 – 7338	8	1200	phot	2″	CRAF
	1992	Apr	9	7085 – 9864	2	3600		2″	CRAF
	1992	Apr	9	7085 – 9864	6	1800	phot	2″	CRAF
3C263	1992	Dec	31	4580 – 7297	7.5	1200	phot	2″	TI
	1992	Jan	2	6264 – 8998	5	1200	phot	2″	TI
	1992	Jan	2	6264 – 8998	2	1200		2″	TI
	1992	Jan	3	6264 – 8998	2	1800	cloud	2″	TI
	1992	Jun	1[f]	7090 – 8506	2	3600	cloud		CRAF
	1992	Jun	7[f]	7168 – 8588	2	3600	cloud	1″	CRAF
3C277.1	1991	Dec	31	4580 – 7297	7.5	1200	phot	2″	TI
	1992	Jan	1	4557 – 7275	2	2100		2″	TI
	1992	Feb	26[e]	4939 – 9500	2.4	3000		2–3″	TI
	1992	Feb	28[f]	5796 – 7201	2	2700		2–2.5″	TI
	1992	Feb	29[f]	6305 – 7694	2	5400		2–2.5″	TI
	1992	Mar	11	3099 – 5814	2	2700		2″	TI
3C323.1	1992	Apr	7	4583 – 7338	2	3600		1.5″	CRAF
	1992	Apr	7	4583 – 7338	8	900	phot	1.5″	CRAF
	1992	Apr	9	7085 – 9864	2	3600		1.5″	CRAF
	1992	Apr	9	7085 – 9864	6	1200	phot	1.5″	CRAF

[a] Nominal wavelength range. Quality may have deteriorated below 3250 Å and above 9000 Å.

[b] Phot = photometric, approximate seeing (FWHM) is given.

[c] Notes: For TI CCD: thinned, 15 μm pixels. For CRAF CCD: thick, 12 μm pixels.

[d] 3C 175: Spectrum optimally extracted using an aperture truncated where the point profile intersects the nearby star profile, a point generally at the 1/3 peak level.

[e] These observations were made at KPNO; all others from McDonald Observatory.

[f] These higher resolution observations were made for a related program to investigate Hβ line profiles.

from Massey et al. 1988 and Massey & Gronwall 1990) observed at the same air mass.

Additional spectra were taken at the KPNO 2.1 m telescope on 1992 February 26. A thinned Ford 3K × 1K CCD was used with the Gold Camera spectrograph to obtain 6 Å resolution spectra of 3C 277.1 and 3C 215 over the wavelength range 4939–9500 Å. Observations of five different standard stars allowed the determination of the relative flux as a function of wavelength to an accuracy of ~5%, but all data were taken through a 2″.4 slit and thus had an uncalibrated gray shift. Atmospheric absorption has not yet been removed, and large-slit data were obtained on another night but are not yet reduced.

For some spectra, overlapping data from slightly different epochs were combined. The spectra were checked for differences between epochs. No significant differences were found, but in any case this is unlikely to be important for the strengths of the narrow lines of interest here. For most optical data obtained under photometric conditions the match of overlapping FOS and optical spectra was excellent and required no scaling. Some optical data obtained under nonphotometric conditions were scaled to match the overlapping FOS spectra.

3. ANALYSIS AND RESULTS

Examples of combined *HST*–ground-based spectra, showing the wide wavelength coverage, are given in Figure 1. We note regions affected by atmospheric absorption. The

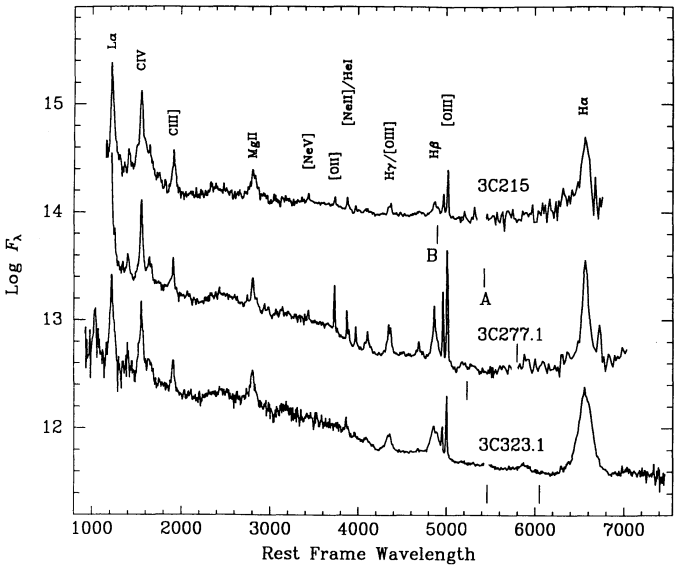

FIG. 1a

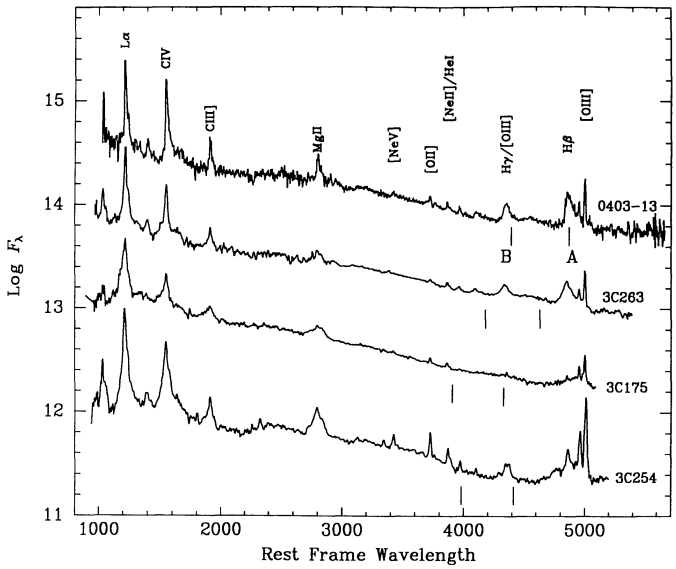

FIG. 1b

FIG. 1.—Sample *HST*-McDonald-KPNO spectra illustrating the wide wavelength coverage. The ordinate is plotted on displaced scales, and data have been smoothed for display. The vertical bars indicate positions of atmospheric *A*- and *B*-band absorption that have been divided out in the McDonald data, and omitted from the long-wavelength spectra of 3C 215, 277.1, and 323. 1 (*A*-, *A*-, and *B*-band respectively).

spectra have been corrected for Galactic reddening using the empirical function derived by Cardelli, Clayton, & Mathis (1989, in IRAF) and $E(B-V)$ from Burstein & Heiles (1982, and private communication). Except for one quasar, 3C 215, which has an unusually flat continuum, the continuum shapes agree very well. This is true even for the two quasars at low Galactic latitude, PKS 0403−13 and 3C 175, suggesting that uncertainties in Galactic reddening do not result in significant uncertainties in their ultraviolet line intensity ratios.

The fluxes of all narrow lines, together with estimated errors, are given in Table 2. The uncertainties have been estimated by comparing fluxes derived choosing low and high continuum levels, since uncertainties in defining the continuum are often the dominant source of error. In most cases, the narrow Hβ line is well separated from the broad-line component and the associated uncertainty is small. Weaker lines like [O III] λ4363 and He II λ4686 are strong enough in a few objects to obtain reliable fluxes. Such lines are very useful as density and reddening indicators (see below). However, separation of the narrow Hα component is more complicated because of the nearby narrow lines of [N II] $\lambda\lambda$6548, 6584. In the case of 3C 277.1 we first used [O III] λ5007 to remove the narrow Hβ spike. The residual broad Hβ profile was then used as a template for the broad Hα profile, while [O III] λ5007 furnished the template for narrow Hα and [N II] $\lambda\lambda$6548, 6584. We simultaneously adjusted these four components to give a best fit to the observed blend, maintaining the correct 3:1 intensity ratio between the [N II] lines.

A striking result from our new data is the absence of any strong ultraviolet narrow lines with widths the same as the optical [O III] λ5007 line. The upper limits to the narrow-line components were determined as follows. First, we assume that the [O III] λ5007 profile is appropriate for any narrow lines in the ultraviolet. To first order this is reasonable as we wish to interpret the line ratios in terms of emission from the same physical region or regions. We simply subtract in quadrature the optical instrumental FWHM, as determined from the wavelength comparison spectrum, from the observed width (FWHM) of the strong [O III] λ5007, to derive an intrinsic narrow line width. Even if the quasar image underfills the 2″ slit this should not be a serious source of uncertainty. We then add in quadrature to this intrinsic narrow line width the *HST*-FOS instrumental FWHM appropriate to the particular FOS grating setup. Second, we fit a Gaussian profile of this FWHM (in velocity space) to the peak of the observed ultraviolet broad-line profiles, taking into account that C IV and Mg II are doublets. The intensity of this Gaussian "narrow line" is then an upper limit to the strength of any true narrow line having this profile. Subtraction of this narrow-line profile would result in a flat-topped broad line. Subtraction of the profile of a narrow line of greater intensity would result in a dip in the top of the broad line. This may or may not be physically unreasonable depending on the presence of absorption intrinsic to the quasar and occurring at the same wavelength.

Although we cannot unambiguously measure any narrow-line component to the broad ultraviolet lines, we note that in some cases, there is a tendency for the C III] λ1909 line to be narrower than C IV λ1549. The best illustration of this is 3C 277.1 (Fig. 1) for which the C III] FWHM is only 1800 km s^{-1} compared with 2600 km s^{-1} for C IV and Mg II λ2798. He II λ4686 is also significantly narrower than C IV λ1549 in this quasar. This is interesting because, of the spectra presented here, that of 3C 277.1 has the strongest optical narrow lines.

Figure 2*a* shows examples of the subtraction of narrow lines of intensity equal to these upper limits and Table 2 lists all upper limits thus obtained. A problem with this procedure arises in the three cases where significant associated absorption occurs near the peak of the line (3C 254, 277.1, and 323.1). We attempt to estimate where the line profile may have been in the absence of absorption. This is very uncertain as the widths and wavelengths of absorption features may be similar to those of narrow lines. Figure 2*b* illustrates the broad-line profiles as they would appear with the addition of a narrow-line com-

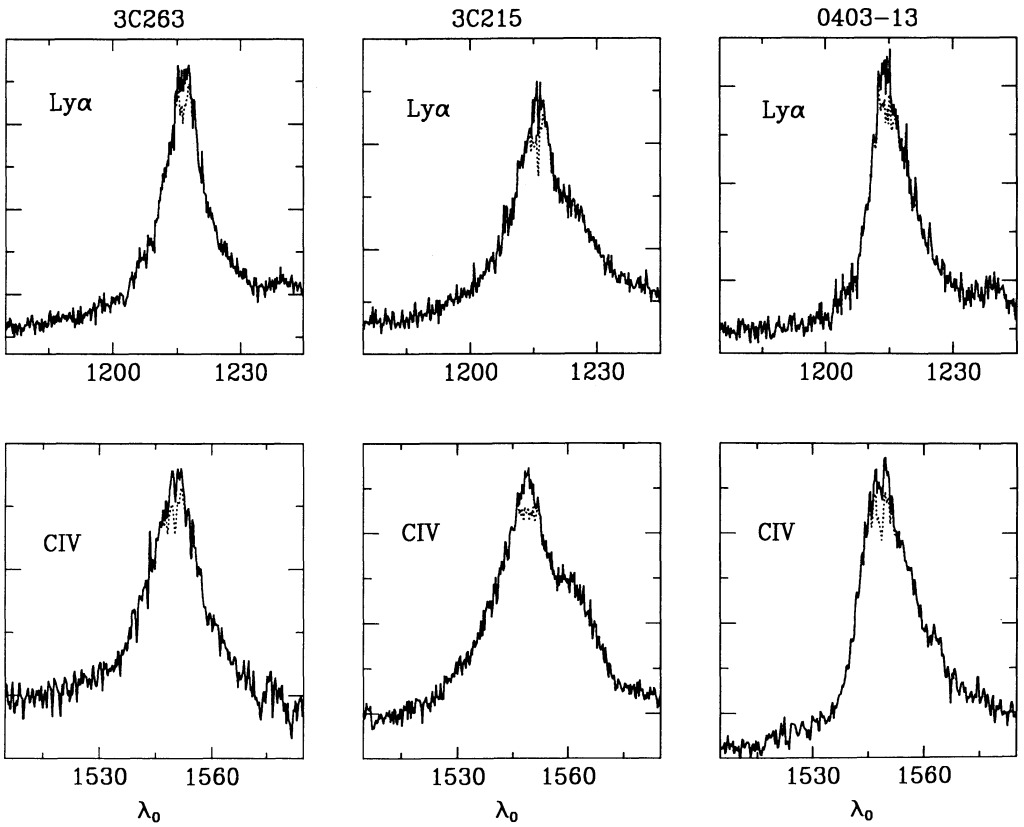

FIG. 2*a*

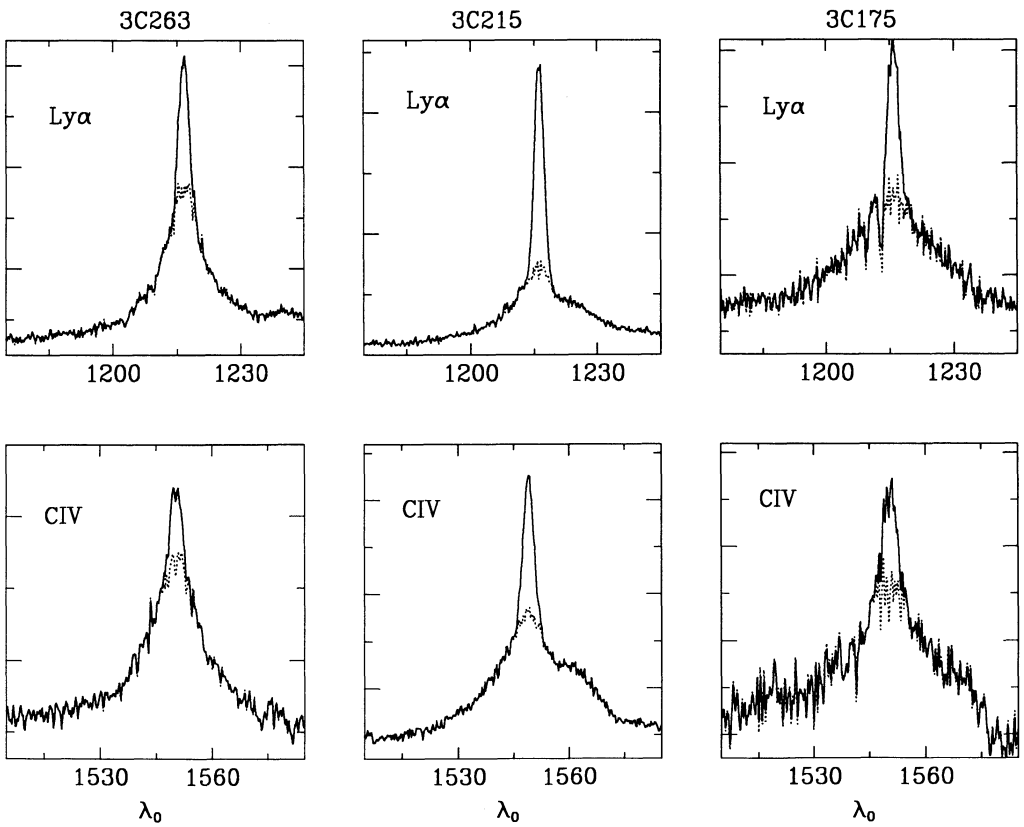

FIG. 2*b*

FIG. 2.—(*a*) Examples of the observed Lyα and C IV λ1549 profiles (*solid lines*) minus the narrow line profiles (*dotted lines*), using the estimated upper limits of Table 2, and corrected for the instrumental resolutions. (*b*) Expected appearance of line profiles of Lyα and C IV λ1549 based on the observed broad line profile (*dotted lines*) combined with the predicted narrow-line component based on the reddening-corrected Seyfert 2 spectrum of Table 3. The instrumental resolution of the optical and UV data has been taken into account, as explained in the text.

TABLE 2
FLUXES OF THE NARROW LINES[a]

Line	0403-13		3C175		3C215		3C254		3C263		3C277.1		3C323.1	
E(B-V)[b]	0.024		0.186		0.024		0.020		0.00		0.00		0.034	
z	0.571		0.768		0.411		0.734		0.652		0.320		0.264	
FWHM[OIII] (km s^{-1})	570		675		500		670		526		530		498	
O VI λ1035	...		...		...		...		< 5		...		<13	
Lα	<7.8		< 8.7		<4.4		<17		<14		<4.5		<40	
1400	...				...		...		...		...		...	
C IV λ1549	<5.8		< 2.6		<2.1		< 3.6		<8.8		<3.2		<13.0	
He II λ1640	...		...		...		...		<5.0		≤1.3		<2.3	
C III] λ1909	<2.4		< 2.9		<0.86		< 2.2		<3.0		<2.8		<2.7	
Mg II λ2798	<1.0		5.0,3.0[c]	±1.	<1.1:		1.35	±0.3	<2.8		<1.4		<6.0	
Ne IV?λ3342	...		...				1.4	±0.3	...					
[Ne V] λ3426	2.0	±1.0	...		2.4	±0.6	1.8	0.5	3.0	±0.7	...		...	
[O II] λ3727	1.5	0.5	2.9	±0.7	2.2	0.4	3.8	0.4	4.0	0.5	12.0	±0.5	6.8	±1.2
[Ne III] λ3869	1.5	0.5	3.3	0.6	3.6	0.6	2.6	0.3	3.5	0.8	4.75	0.1	0.9	0.2
[Ne III] λ3967	1.9	0.6	...		1.5	0.5	1.2	0.2	2.5	1.0	2.6	0.5	4.0	0.7
Hδ	...		...		...		1.0	0.2	...		1.4	0.3	...	
Hγ	...		...		...		...		1.6	0.4	1.8	0.3	...	
[O III] λ4363	0.9	0.03	1.2	0.3	1.2	0.3	0.6	0.2	1.3	0.5	1.6	0.2	2.7	1.0
He II λ4686	<0.3		1.1	0.3	1.5	0.6	1.05	0.1	1.5	0.6	1.1	0.2	1.05	0.1
Hβ	2.4	0.4	1.4	0.3	0.6	0.2	2.0	0.5	2.5:	0.3	5.0	0.5	5.0	1.0
[O III] λ4959	3.5	0.7	5.8	1.0	4.5	0.5	7.0	0.6	5.7	0.7	12.1	0.3	12.5	0.3
[O III] λ5007	11.8	0.1	15.0	1.0	13	0.6	19.7	0.9	23.0	1.0	37.0	0.2	44.0	0.7
FeVII λ6087	...		...		...		...		...		...		1.2	0.3
[O I] λ6300	...		...		...		...		...		...		1.3	0.4
Hα	...		...		...		...		...		22.0	±4.5	13.0	2.0
[N II] λ6548, 6584	...		...		...		...		...		13:		...	

[a] Line fluxes are in units of 10^{-15} ergs s^{-1} cm^{-2}, and effectively through a 2″ × 2″ slit. A direct comparison of wide and narrow slit fluxes yielded no significant differences except for [O II] λ3727 in 3C 254: $(3.8 \pm 0.5) \times 10^{-15}$ (narrow), and $(6.3 \pm 1.0) \times 10^{-15}$ ergs s^{-1} cm^{-2} (broad slit). The latter were measured from the April data, but the January data show this difference too.

[b] The values in this table are corrected for reddening, using Galactic $E(B-V)$ kindly provided by D. Burstein (private communication).

[c] The narrow line was measured in two ways, one with the peak wavelength displaced from the predicted value.

ponent. The latter is taken from the typical (reddening corrected) Seyfert 2 spectrum presented in Table 3. Clearly, we do not see lines even nearly as strongly peaked as these.

4. DISCUSSION

4.1. *The Narrow-Line Spectrum*

No narrow component of any ultraviolet broad emission line could be identified unambiguously. All our ultraviolet measurements are upper limits despite the fact that most optical narrow lines are strong and well defined. This indicates that some form of line destruction is taking place. For illustration, in Table 3 we compare the observed line ratios with the results of photoionization calculations designed to reproduce the observed optical narrow-line spectrum. The calculations are performed by the codes CLOUDY and ION (see Rees, Netzer, & Ferland 1989 for details and more references). We

TABLE 3
COMPARISON OF NARROW-LINE RATIOS WITH THEORETICAL MODELS

Line	0403-13	3C175	3C215	3C254	3C263	3C277.1	3C323.1	Sey 2[a]	Typical quasar[a]	N=10^6 cm^{-3} U=3.4 × 10^{-3}	N=10^4 cm^{-3} U=3.4 × 10^{-5}
Lα	<3.3	<6.2	<7.3	<8.5	<5.6	<0.9	<10	55	<7	37	27
Hα	·	·	·	·	·	4.4	2.6	3.1	3	3	2.7
Hβ	1	1	1	1	1	1	1	,1	1	1	1
He II λ4686	·	·	·	·	0.6	0.22	0.21	0.29	0.2	0.19	0.07
He II λ1640	·	·	·	·	<2.0	≤0.26	<0.46	·	< 0.5	1.3	0.4
[O III] λ5007	4.9	10.7	21.7	9.9	9.2	7.4	8.8	10.8	9	12	0.06
[O III] λ4363	0.38	·	2.0	0.3	0.5	0.32	0.54	0.21	0.4	0.7	·
[O II] λ3727	0.63	2.07	3.7	1.9	1.6	2.40	1.4	3.2	2	0.06	5
[O I] λ6300			·	·	·	·	0.26	0.57	0.3	0.3	2.0
[Ne III] λ3967	0.79	·	2.5	0.6	1.0	0.52	0.8	·	1	2.4	0.5
Mg II λ2798	<0.4	3.6,2.1	<1.8:	≤ 0.7	<1.1	<0.28	<1.20	1.8	<0.7	6	4
C III] λ1909	<1.0	<2.1	<1.4	<1.1	<1.2	<0.56	<0.54	5.5	<1	3.3	0.03
C IV λ1549	<2.4	<1.8	<3.5	<1.8	<3.5	<0.64	<2.6	12.	<2	1.4	·
R_{NLR}(Kpc)[b]	3.7	4.1	3.3	4.0	3.9	2.9	2.5			0.035–0.17	3.5–17

[a] Mean Seyfert 2 spectrum after Galactic and internal reddening correction (FO86). The quasar spectra have been corrected only for Galactic reddening.

[b] For the individual quasars, the linear distance in the sky plane corresponding to a slit center-to-edge size of 1″ is given for comparison with NLR distances deduced from the models. We used $H_0 = 100$ km s^{-1} Mpc^{-1}, $q_0 = 0.5$.

take a "standard" AGN continuum, as suggested by Mathews & Ferland (1987), and solar composition for the heavy elements. Our spectra show strong high-excitation (e.g., [O III] λ5007) and low-excitation lines (e.g. [O II] λ3727) and there are indications of relatively high densities (strong [O III] λ4363 emission compared with [O III] λ5007). We therefore show two different models, spanning a range of 100 in ionization parameter and gas density. As an example, these could be viewed as two points (i.e., two individual optically thick clouds; see a general description in Netzer 1990) in a large, extended atmosphere where the density drops as R^{-1} and the ionization parameter decreases outward as $U \propto R^{-1}$.

As is evident from Table 3, it is possible to fit the observed optical narrow lines with a combination of these models but none resembles the observed ultraviolet narrow-line spectra. Table 3 also compares our (mean) observed line ratios with typical values found for the nuclei of Seyfert 2 and NLRGs, corrected for Galactic and intrinsic reddening (FO86). The narrow-line spectra of our high-luminosity AGNs are quite different from the dereddened spectra of the lower luminosity objects. Lyα is a factor of 5–10 underluminous compared with Hβ, and Mg II λ2798 is very weak too. The lines of C IV λ1549 and C III] λ1909 are weak compared with a typical unreddened Seyfert 2 spectrum but are still consistent with some models.

The spectra of some of our objects show the line of He II λ4686, which when combined with the upper limit to He II λ1640, gives a direct lower limit to the amount of reddening. The theoretical intensity ratio He II λ1640/He II λ4686 is between 6 (low-density limit, Seaton 1978) and about 11 (high-density limit, Hummer & Storey 1987) and we do not expect complications caused by line opacity. From Table 2 we find observed narrow-line ratios of less than 3.3 (3C 263), less than 1.2 (3C 277.1), and less than 2.2 (3C 323.1). The quasar 3C 277.1 is the most interesting, not just because it has the smallest upper limit, but because of the especially narrow He II λ1640 line, where the ratio may represent a real measurement, ~ 1. This would correspond to reddening by external dust equivalent to $E(B-V) = 0.5 \pm 0.1$, which is in good agreement with the value $E(B-V) \simeq 0.4$ implied by the observed Balmer decrement (Hα/Hβ = 4.4). A naive interpretation would suggest, therefore, that there is no difference between these QSOs and typical Seyfert galaxies once the quasar spectra have been properly corrected for external reddening.

However, the other object in our sample for which we have a good narrow Hα line measurement (3C 323.1) shows very different behavior—the Hα/Hβ ratio is nearly case B while all of the UV lines are very weak compared with our models. This has at least the superficial appearance of being the signature of *internal* reddening. In fact, Kinney et al. (1991) have found similar behavior for some Seyfert galaxies observed with *IUE*. This prompts us to investigate in greater detail the predicted hydrogen line spectrum for the two types of reddening.

4.2. *The Hydrogen Narrow-Line Spectrum*

We used the program CLOUDY to calculate the predicted behavior of the most important emission lines, and particularly of Lyα/Hβ versus Hα/Hβ, for two limiting cases. One case is reddening by grains external to the emission-line regions, while the other is extinction within the line-forming region by embedded grains. These, or a combination of the two effects, are the only possible causes for the narrow-line Lyα/Hβ ratios to be so far below that expected from case B assumptions.

We have made a series of photoionization calculations in which a constant density gas ($n_H = 10^5$ cm^{-3}) was irradiated by the generic AGN continuum mentioned earlier. It is clear that the NLR is actually composed of gas with a wide range of density and ionization (Filippenko and Sargent 1988), but the results we are concerned with here (the hydrogen-line spectrum and the intensities of the ultraviolet lines) do not depend strongly on the gas density. They are instead more sensitive to the ionization parameter U, the metallicity, and the possible presence of grains.

The results of the calculations are shown in Figure 3. The upper panel shows predictions for the case of a grain-free solar composition for the 15 elements included in the calculation (Grevesse & Anders 1989). The behavior of the lines is fairly conventional—low-ionization lines weaken, and high-ionization lines grow stronger, as U increases. Recombination line intensities do not depend on U so the predicted Lyα/Hβ and He II λ4686/Hβ ratios do not change. The Hα/Hβ ratio is not plotted but remains close to the case B prediction of 2.8. The Lyα/Hβ ratio is nearly an order of magnitude larger than observed.

The lower panel shows similar calculations but including the effects of internal dust. We have assumed that both the properties of the dust grains and the depleted gas-phase abundances are like those in the local interstellar medium (ISM). In particular, the grains have an ISM ratio of total to selective extinction, and both graphite and an astronomical silicate component are included using the computational methods described in Baldwin et al. (1991). The depleted ISM abundances are taken from Cowie & Songaila (1986). The elements He, C, N, O, Ne, Na, Mg, Al, Si, S, Ar, Ca, Fe, and Ni are

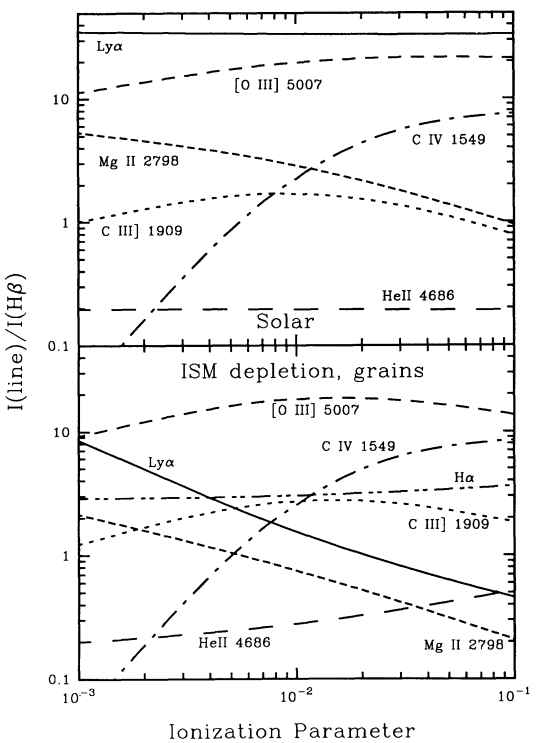

FIG. 3.—A series of photoionization calculations showing the spectrum of a dust-free NLR cloud (*upper panel*) and the one expected from a dusty cloud with ISM composition of the heavy elements (*bottom*). The line intensities relative to Hβ are shown as a function of the ionization parameter U. For more information see the text.

assumed to have abundances (by number relative to hydrogen) given by 0.098, 2.51(−4), 7.94(−5), 5.01(−4), 1.23(−4), 3.16(−7), 1.26(−5), 7.94(−8), 3.16(−6), 3.24(−5), 2.82(−6), 1.00(−8), 6.31(−7), 1.82(−8).

The predicted spectrum shown in the lower panel is what would be seen by an observer viewing the illuminated face of the cloud; for the case of an irradiated molecular cloud this would be the only side from which emission lines would escape. This spectrum includes the effects of grains on line transfer, and (for optically thin lines) the destruction during the single flight escape from the illuminated face.

The results of the lower panel of the figure can be understood in terms of a competition between gas and dust for ionizing radiation. The ionization parameter is related to the level of ionization of the gas at the illuminated face of the cloud. Thus the hydrogen opacity decreases with increasing U, but the grain opacity remains constant (assuming that the grains survive). Therefore increasing U also increases the probability that an incident ionizing photon will be absorbed by dust rather than by gas. As a result, the dust extinction of the observed line spectrum becomes larger as U increases. This accounts for the weakening of Lyα/Hβ, and the increase of the Balmer decrement Hα/Hβ, as U increases. The relative strengthening of He II λ4686, on the other hand, is the result of a change in the ionization structure caused by the selective removal of lower energy ionizing radiation by the dust in the ionized region (Aannestad 1989).

We do not concentrate on the intensities of the ultraviolet emission lines since these depend strongly on the temperature of the gas (because of their large Boltzmann factors), making their intensities sensitive to the global metallicity of the gas and the form of the ionizing radiation field. In particular we do not explore the effects of the mild chemical enrichments that are likely to be present on kiloparsec scales in giant elliptical galaxies (see, for example, Efstathiou & Gorgas 1985).

Figure 4 shows the predicted hydrogen line ratios, both for the case of solar abundance gas (without grains) and for the internally reddened ISM mixture. For the internally reddened case the line of increasing ionization parameter goes downward and to the right as the hydrogen spectrum is extinguished by ever increasing amounts. For the largest values of U the Hα/Hβ ratio is larger and the Lyα/Hβ ratio smaller than expected in the absence of dust.

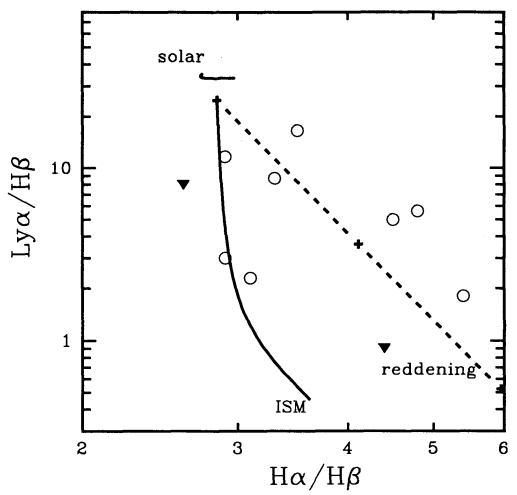

FIG. 4.—Observed and predicted hydrogen line ratios. The ISM line shows the calculated intensity for an increasing ionization parameter (lowest value at the top). The reddening curve shows the effect of dust along the line of sight. Lines of increasing reddening are straight lines parallel to the one shown that can be drawn from any point on the ISM curve (e.g., from the top, where there is no internal dust). The observations are from Kinney et al. (1991, *open circles*). Upper limits to the ratio Lyα/Hβ, from the present measurements, range from 1 to 8, and the two quasars with measured Hα/Hβ are shown as filled triangles (3C 277.1 and 3C 323.1).

Figure 4 also shows a simple reddening line assuming external extinction due to intervening galactic grains with no scattered light returned to the path toward the observer. We use the average extinction curve given by Osterbrock (1989, his Table 7.2 and eq. [7.6]). The two crosses mark extinctions corresponding to $c = 1$ and $c = 2$. Figure 4 is a log-log plot, so lines of increasing reddening are straight lines that can be drawn away from any point on a predicted spectrum, including from points on the line corresponding to internally reddened cases. The observed points in Figure 4 that correspond to Seyfert 2 galaxies are taken from Kinney et al. (1991), while the two points corresponding to the narrow lines of broad-lined objects are taken from the present work.

It is clear that many of the narrow-lined objects have intrinsic spectra that are reddened away from either the solar case or the case of ISM photoionization with a low ionization parameter, with most of the effect coming from external reddening. However, the spectra of 3C 323.1 in our sample and of two objects from the Kinney et al. sample appear to have relatively low external reddening but could be explained by internal reddening, i.e., the emission lines originate in dusty (ISM) clouds of high-ionization parameter. Assuming that the gas producing the narrow lines is basically the same in the different objects, we are led to the conclusion that the NLR in these latter three objects is relatively high-density gas containing grains, but with a very wide range in the ionization parameter (producing a wide range in the Lyα/Hβ ratio). Kinney et al. noted the problem and concluded, without actually calculating models, that internal dust is a likely explanation. A similar conclusion was reached by Ferland (1992), who noted that calcium must be highly depleted in NLR gas.

4.3. *The NLR Size*

The models shown can be used to deduce the dimensions of the NLR in the objects under study. These are listed in Table 3 as a range of radii for the two models, where the smallest and the largest sizes correspond to the lowest (3C 215) and highest (3C 175) luminosity objects. For comparison, the size of a typical Seyfert 1 galaxy, deduced from such models, is between 20 and 1000 pc. The observation of low-ionization lines, especially those sensitive to collisional de-excitation like [O II] λ3727, require the largest NLRs. Thus, the NLR in high-luminosity AGNs extends far from the nucleus and in some cases its extent could approach the size of the galaxy. This scale can be resolved by ground-based and space observations, and the narrow emission lines that we observe may be related to the nebulosity seen in several high redshift quasars (e.g., Heckman et al. 1991a; Bremer et al. 1992, and references therein). Note, however, that at least some of this extended emission-line gas may be ionized by a continuum beamed away from our line of sight. There is a significant tendency for the extended NLR emission of quasars to be aligned along the radio jet or lobe direction (Stockton & MacKenty 1987; Baum & Heckman 1989a, b; Heckman et al. 1991b). This tendency is even stronger in the radio galaxies, whose axes probably lie closer to the sky plane. Our quasars are classical radio-loud

AGNs, and except for PKS 0403−13, are very lobe-dominated. Thus the ionizing continuum seen by the NLR may be stronger—and not the same shape as assumed in our calculations.

5. CONCLUSIONS

We have presented the first systematic study of the narrow emission lines in high-luminosity AGNs. Our FOS *HST* observations, when combined with our ground-based data, provide very wide coverage of the spectra of seven radio-loud quasars and allow the measurement of a large number of lines. We have shown and discussed only the narrow lines, and compared them with those observed in Seyfert 2s and NLRGs. Our upper limits to the fluxes of the ultraviolet lines assume that they are not broader than the [O III] λ5007 line. The real situation may be more complex if line widths depend on ionization parameter or critical density (e.g., van Gröningen 1992; Osterbrock 1991), so this should be kept in mind. Our interpretation of the data using photoionization calculations suggests that all ultraviolet lines are affected by the presence of dust. In some objects the spectrum is consistent with a line-of-sight reddening, presumably in the host galaxy of the quasar. In others, the observed hydrogen line ratio excludes such a simple interpretation and we suggest that the small Lyα/Hβ intensity ratio is a result of internal dust in the NLR clouds. We also show that the NLR in such objects may extend at least several kiloparsecs from the nucleus. The single most important observational result is that the high-luminosity AGNs in this sample do not show any sign of narrow ultraviolet lines with Doppler widths like those seen in their optical spectra.

We are very grateful to David Doss, Al Krebs, and Doug Otoupal for willing instrumental help at the McDonald Observatory. Anne Kinney, George Hartig, Daniel Golombek, Tony Keyes, Jen Christiansen, and their colleagues at STScI suffered innumerable questions, and their patience is much appreciated. Dianne Harmer and Jeannette Barnes were especially helpful for the KPNO observations. H. N. thanks the director and staff of CTIO for their hospitality and help during a 2 month sabbatical visit to CTIO. B. J. W. and D. W. thank the National Science Foundation for partial support of the ground-based part of this work (NSF AST 8714937). G. J. F. acknowledges support under a National Science Foundation grant, NSF AST 9019692. The *Hubble Space Telescope* part of this work was supported by grant no. HST GO-2578.01-87A RQ-Q from the Space Telescope Science Institute, which is operated by AURA, Inc., under NASA contract NAS5-26555. We also thank the US-Israel Binational Science Foundation for support (BSF 8900179).

REFERENCES

Aannestad, P. A. 1989, ApJ, 338, 162
Antonucci, R. R. J. 1992, in Testing the AGN Paradigm, ed. S. Holt, S. Neff, & C. M. Urry (New York: American Institute of Physics), 486
Baldwin, J., Ferland, G., Martin, P., Corbin, M., Cota, S., Peterson, B., & Slettebak, A. 1991, ApJ, 374, 580
Baum, S. A., & Heckman, T. 1989a, ApJ, 336, 681
———. 1989b, ApJ, 336, 702
Bremer, M. N., Crawford, C. S., Fabian, A. C., & Johnstone, R. M. 1992, MNRAS, 254, 614
Burstein, D., & Heiles, C. 1982, AJ, 87, 1165
Carswell, R. F., et al. 1991,ApJ, 381, L5
Cardelli, J. A., Clayton, G. C., & Mathis, J. S. 1989, ApJ, 345, 245
Clavel, J., & Wamsteker, W. 1987, ApJ, 320, L9
Cowie, L. L., & Songaila, A. 1986, ARA&A, 24, 499
Efstathiou, G., & Gorgas, J. 1985, MNRAS, 215, 37P
Ferland, G. J. 1993, in Proc. of the Madrid meeting, The Nearest Active Galaxies, ed. J. E. Beckman, L. Colina, & H. Netzer (Madrid: CSIC)
Ferland, G. J., & Netzer, H. 1979, ApJ, 229, 274
Ferland, G. J., & Osterbrock, D. E. 1986, ApJ, 300, 658 (FO86)
Filippenko, A., & Sargent, W. L. W. 1988, ApJ, 324, 134
Ford, H. C., & Hartig, G. F. 1990, Faint Object Spectrograph Handbook, Version 1.1 (Baltimore: STScI)
Grevesse, N., & Anders, E. 1989, in Proc. AIP Conf. 183, Cosmic Abundances of Matter, ed. C. J. Waddington (New York: AIP), 1
Heckman, T. M., Lehnert, M. D., Miley, G. K. & van Breugel, W. 1991a, ApJ, 381, 373
Heckman, T. M., Lehnert, M. D., van Breugel, W., & Miley, G. K. 1991b, ApJ, 370, 78
Hummer, D. G., & Storey, P. J. 1987, MNRAS, 224, 801
Kinney, A. L. 1992, Faint Object Spectrograph Handbook, Version 2.0 (Baltimore: STScI)
Kinney, A. L., et al. 1991, ApJ, 377, 100
Kormendy, J., & Sanders, D. B. 1992, ApJ, 390, L53
Kriss, G. A., et al. 1992, ApJ, 392, 485
MacAlpine, G. M. 1985, Astrophysics of Active Galaxies and Quasi Stellar Objects, ed. J. S. Miller (Mill Valley CA: University Science Books), 259
Massey, P., & Gronwall, C. 1990, ApJ, 358, 344
Massey, P., Strobel, K., Barnes, J. V., & Anderson, E. 1988, ApJ, 328, 315
Mathews, W. G., & Ferland, G. J. 1987, ApJ, 323, 456
Netzer, H. 1982, MNRAS, 198, 589
———. 1990, in Active Galactic Nuclei, ed. T. J.-L. Courvoisier & M. Mayor (Berlin: Springer), 57
Netzer, H., Wills, B. J., & Wills, D. 1982, ApJ, 254, 489
Osterbrock, D. E. 1989, Astrophysics of Gaseous Nebulae & Active Galactic Nuclei (Mill Valley, CA: University Science Books)
———. 1991, Rep. Prog. Phys., 54, 579
Rees, M., Netzer, H., & Ferland, G. J. 1989, ApJ, 347, 640
Rowan-Robinson, M. 1977, ApJ, 213, 635
Seaton, M. J. 1978, MNRAS, 185, 5P
Stockton, A., & MacKenty, J. 1987, ApJ, 316, 584
van Gröningen, E. 1992, A&A, in press